

## **Supporting Information**

### **Primary and Rechargeable Zinc-Air Batteries Using Ceramic and Highly Stable, TiCN as Oxygen Reduction Electrocatalyst**

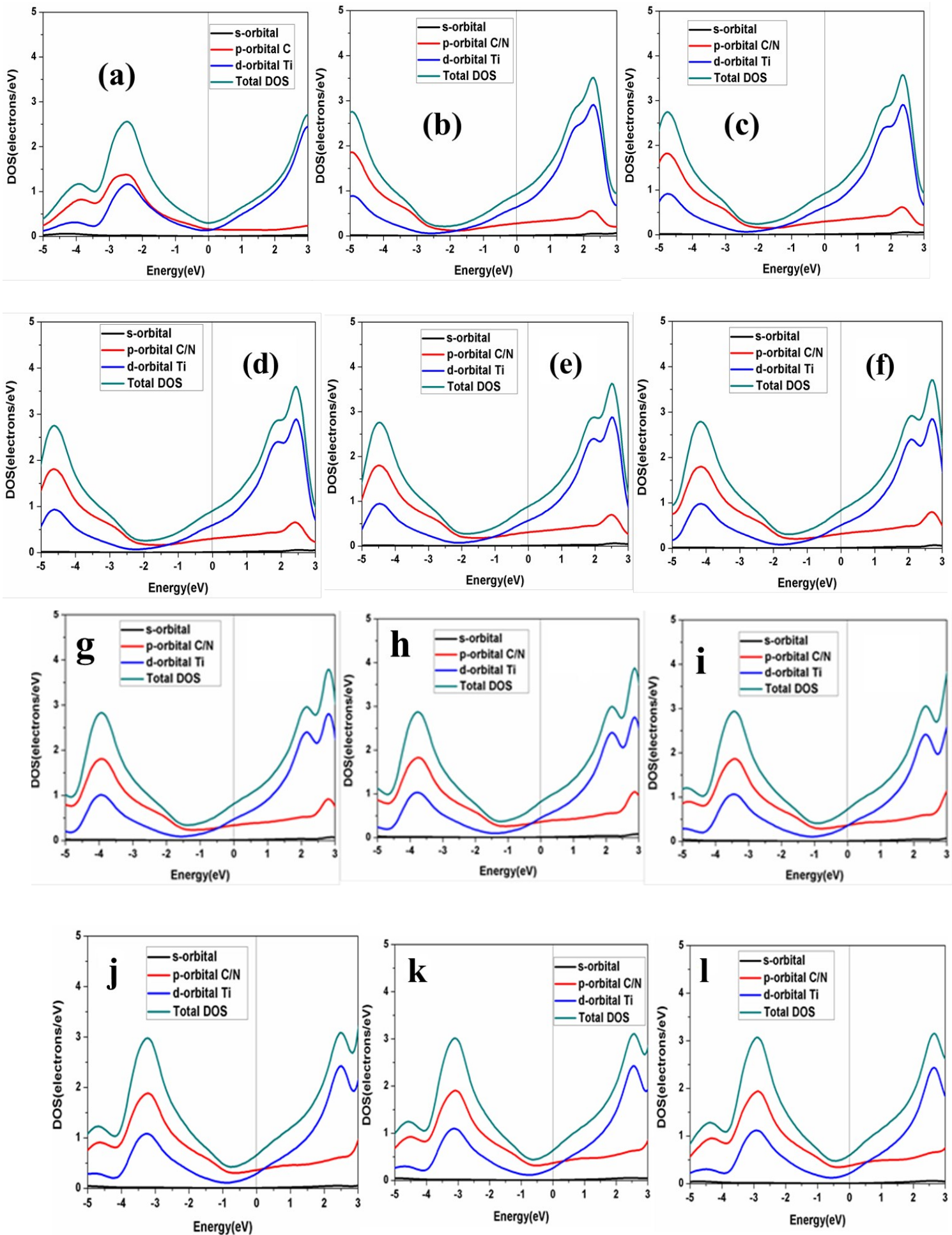
V. G. Anju, R. Manjunatha, P. Muthu Austeria and S. Sampath\*

Department of Inorganic and Physical Chemistry, Indian  
Institute of Science, Bangalore 560012, India

**Table S-1: Composition of TiCN phases, bond lengths and the lattice parameters obtained using DFT calculations.**

S.NO	Phases (GGA/PBE(24x24x24))	Latticeparameters a=b=c	Ti - C/N bond
1	TiN	3.002762	2.12327
2	TiC <sub>0.1</sub> N <sub>0.9</sub>	3.004901	2.12676
3	TiC <sub>0.2</sub> N <sub>0.8</sub>	3.007688	2.12479
4	TiC <sub>0.25</sub> N <sub>0.75</sub>	3.009457	2.12801
5	TiC <sub>0.3</sub> N <sub>0.7</sub>	3.01149	2.12944
6	TiC <sub>0.4</sub> N <sub>0.6</sub>	3.01651	2.13299
7	TiC <sub>0.5</sub> N <sub>0.5</sub>	3.022601	2.13730
8	TiC <sub>0.6</sub> N <sub>0.4</sub>	3.028962	2.14180
9	TiC <sub>0.7</sub> N <sub>0.3</sub>	3.036068	2.14682
10	TiC <sub>0.75</sub> N <sub>0.25</sub>	3.040359	2.14896
11	TiC <sub>0.8</sub> N <sub>0.2</sub>	3.04466	2.15290
12	TiC <sub>0.9</sub> N <sub>0.1</sub>	3.053238	2.15897
13	TiC	3.062686	2.165

Castep package allows to model disorder crystal structure by defining mixture of atoms. **Non-local** corrected generalized gradient approximation based on the Perdew–Burke–Ernzerhof (PBE) formulation was used for optimization.<sup>1</sup>



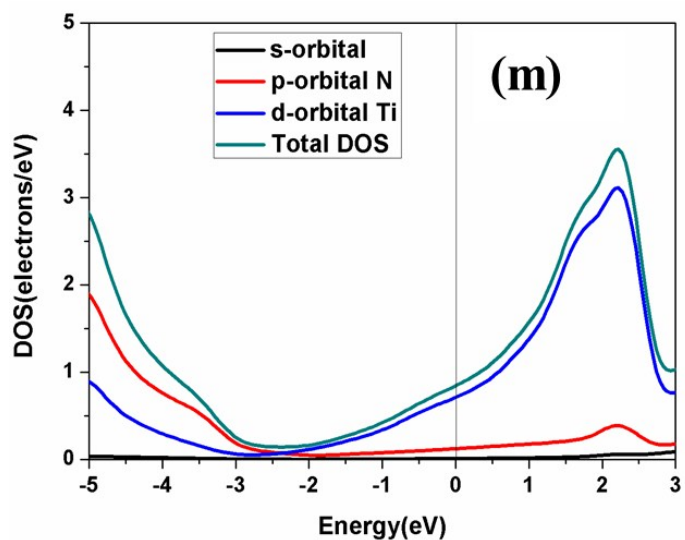
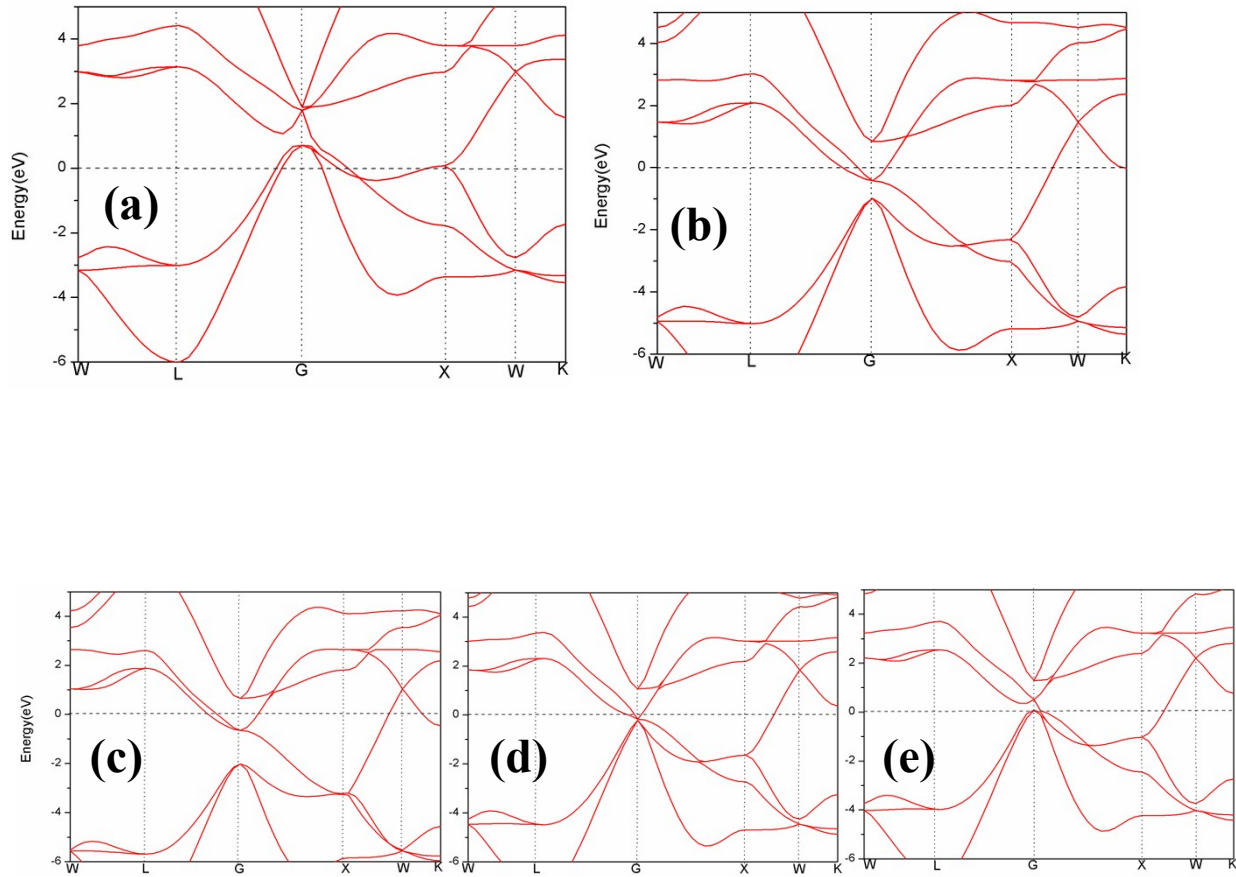


Figure S-1. The computed partial density of states along with total DOS and symmetrically different colours shown for different orbitals. (a)TiC (b)  $\text{TiC}_{0.1}\text{N}_{0.9}$  (c)  $\text{TiC}_{0.2}\text{N}_{0.8}$  (d)  $\text{TiC}_{0.25}\text{N}_{0.75}$  (e) $\text{TiC}_{0.3}\text{N}_{0.7}$  (f)  $\text{TiC}_{0.4}\text{N}_{0.6}$  (g)  $\text{TiC}_{0.5}\text{N}_{0.5}$  (h)  $\text{TiC}_{0.6}\text{N}_{0.4}$  (i) $\text{TiC}_{0.7}\text{N}_{0.3}$  (j)  $\text{TiC}_{0.75}\text{N}_{0.25}$  (k)  $\text{TiC}_{0.8}\text{N}_{0.2}$  (l)  $\text{TiC}_{0.9}\text{N}_{0.1}$  (m)TiN.

**Table S-2. The p band of C/N and d band population of Ti atoms at the Fermi for all the phases studied. The values are obtained by the optimized geometry using GGA/PBE method and Monkhorst–Pack k-point set 24x24x24 (0.016Å) for accuracy.**

S.NO	Phases (GGA/PBE(24x24x24))	Fractional p- band filling at the fermi	Fractional d- band filling at the fermi	Total DOS
1	TiN	0.12135	0.704557	0.835942
2	TiC <sub>0.1</sub> N <sub>0.9</sub>	0.278461073	0.644910511	0.931644451
3	TiC <sub>0.2</sub> N <sub>0.8</sub>	0.296913107	0.622416141	0.928320852
4	TiC <sub>0.25</sub> N <sub>0.75</sub>	0.302866949	0.599750137	0.911539709
5	TiC <sub>0.3</sub> N <sub>0.7</sub>	0.308351	0.575172	0.892358
6	TiC <sub>0.4</sub> N <sub>0.6</sub>	0.318965243	0.516938605	0.84407906
7	TiC <sub>0.5</sub> N <sub>0.5</sub>	0.335178634	0.463127763	0.805940666
8	TiC <sub>0.6</sub> N <sub>0.4</sub>	0.358927954	0.44150789	0.808147346
9	TiC <sub>0.69</sub> N <sub>0.31</sub>	0.368923984	0.3779124	0.753514787
10	TiC <sub>0.695</sub> N <sub>0.305</sub>	0.365258703	0.356404242	0.727882369
11	TiC <sub>0.7</sub> N <sub>0.3</sub>	0.365407056	0.355046782	0.726646024
12	TiC <sub>0.71</sub> N <sub>0.29</sub>	0.3623485534	0.3331114994	0.70120538274
13	TiC <sub>0.75</sub> N <sub>0.25</sub>	0.357976	0.287503	0.650368
14	TiC <sub>0.8</sub> N <sub>0.2</sub>	0.368139205	0.264185689	0.636768148
15	TiC <sub>0.9</sub> N <sub>0.1</sub>	0.372967	0.214158	0.590503
16	TiC	0.161312283	0.136958211	0.300137455



**Figure S-2. Band structures of a) TiC, b) TiN, c)  $\text{TiC}_{0.3}\text{N}_{0.7}$  d)  $\text{TiC}_{0.5}\text{N}_{0.5}$  e)  $\text{TiC}_{0.7}\text{N}_{0.3}$  computed from DFT.**

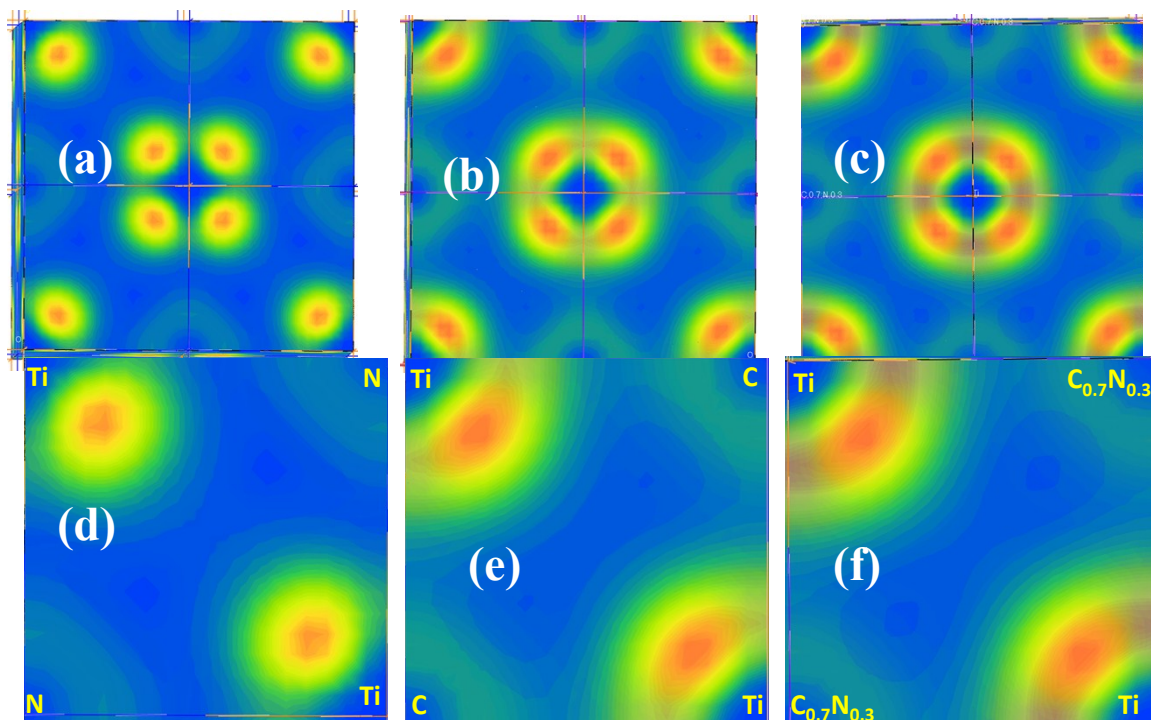
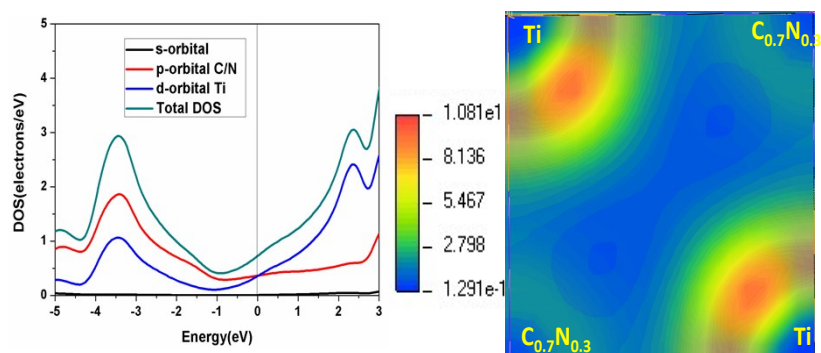


**Figure S-3. Electron density contour plots of a) TiN b) TiC c)  $\text{TiC}_{0.7}\text{N}_{0.3}$ . (d) expanded view of d) TiN e) TiC f)  $\text{TiC}_{0.7}\text{N}_{0.3}$**

The colour codes used are as given in the following figure (Figure 1 in the main text)



**Partial and total DOS of  $\text{TiC}_{0.7}\text{N}_{0.3}$ . The electron density contours for  $\text{TiC}_{0.7}\text{N}_{0.3}$  is also given (right).**

The colour code gives the relative electron density.

The electrocatalytic activity of TiCN towards ORR was assessed by cycling the potential of TiCN nanowire modified glassy carbon electrode in the potential window of 1.1 V to 0.3V vs. RHE at a scan rate of 20 mVs<sup>-1</sup> in 0.5 M KOH which was saturated initially with nitrogen and then with oxygen. In nitrogen saturated electrolyte medium the catalyst shows a pure capacitive behaviour, but oxygen in the medium cause an increase in current at an onset potential of 0.89V vs. RHE as shown in Figure S4 (a). The observed increase in current is due to the reduction of oxygen by the TiCN catalyst. From the effect of scan rate experiment, a linear behaviour (Figure S4 (b)) is observed for the plot of square root of scan rate vs. peak current density as shown in indicating ORR on the catalyst surface is diffusion controlled process as shown in equation 1

$$I_P = -(2.99 \times 10^5) n (\alpha_c n_\alpha)^{1/2} C_0^\infty D_0^{1/2} \nu^{1/2} L \quad (1)$$

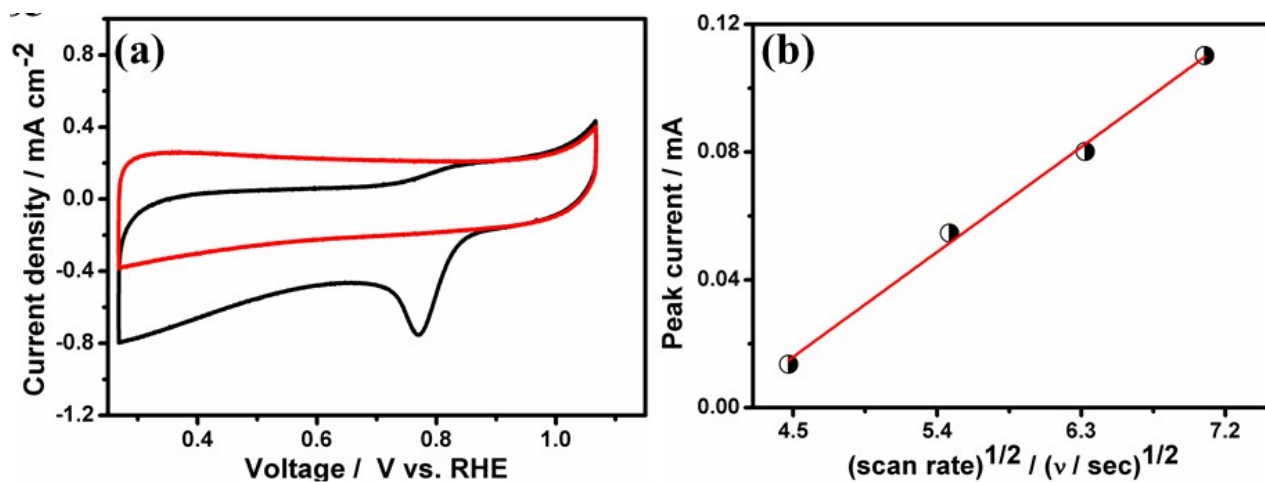


**Figure S-4. (a) Cyclic voltammogram of TiCN nanowire modified glassy carbon electrode in N<sub>2</sub> saturated (red curve) and O<sub>2</sub> saturated 0.5 M KOH. (b) Variation of peak current as a function of square root of scan rate.**

A comparative study for the electrochemical reduction of oxygen on the commercially available TiCN particles over the as prepared TiCN nanowires and Pt/C(had been done by linear sweep voltammetry as shown in Figure S5. The loading of the catalyst were maintained to 0.2 mg / cm<sup>2</sup>. In case of Pt/ C the entire loading of the catalyst was around 0.5 mg/cm<sup>2</sup>, so that the Pt loading (40 wt% Pt on carbon) alone is similar to that of TiCN. Inthe similar experimental conditions the nanowires shows a clear positive shift in the onset potential as compared to that of the nanoparticles.These observations clearly indicate that TiCN nanowires show an upper hand over the nanoparticles for the reaction, both in the thermodynamic and kinetic point of view. Based on the earlier reports we anticipated that the difference in activity observed may be due to the difference in the mode of adsorption of oxygen on the catalytic surface and also due to the difference in the availability of the active plane. Further as the TiCN nanoparticles grows into wires, results in the disappearance of grain boundaries; so as in these one dimensional nanostructure provide an effective and facile pathway for the electrons and the loss due to grain boundaries will be minimum. This can be a cause of high activity observed for the nanowires as compared to particles.

**Table S-3. Comparison of the activity of TiCN catalysts with Pt/C**

<b>Catalyst</b>	<b>Onset potential / V vs. RHE</b>	<b>Half wave potential / V vs. RHE</b>
<b>TiCN particles ( Aldrich)</b>	<b>0.85</b>	<b>0.73</b>
<b>TiCN nanowires (Hydrothermal)</b>	<b>0.89</b>	<b>0.78</b>
<b>40 wt% Pt/ C (Arora Matthey)</b>	<b>0.92</b>	<b>0.8</b>

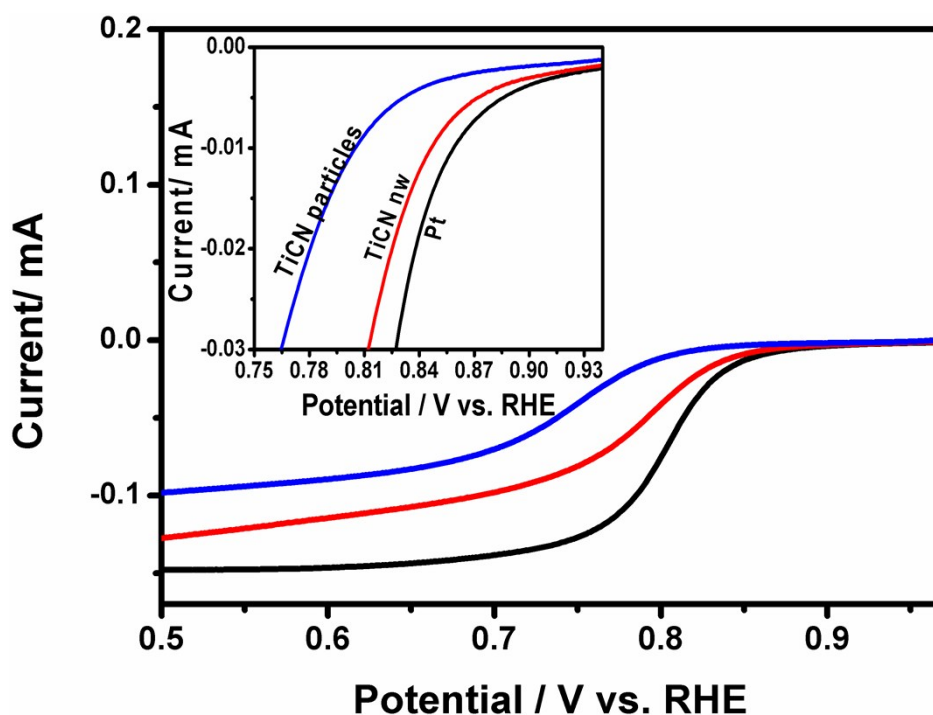


**Figure S-5. Comparison ORR activity for TiCN particle (red curve), nanowires (blue curve) and Pt/C (black curve). Onset potential for ORR on TiCN nanowires is very close to Pt/C as compared to TiCN particles. Inset shows the magnified version to show the onset potential clearly. The loading of the catalyst is not the same since the onset potential is being investigated from this figure.**

The kinetic performance of the catalyst was studied using RDE. From the RDE measurement kinetic parameters were precisely deduced by Koutecky-Levich (Figure S6) as shown in equation 2 and 3. Where,  $i$  is the current density for the potential of interest,  $i_k$  and  $i_d$  are the kinetic and diffusion current density respectively. Further expanding the terms in equation 2 given in equation 3 and in this equation  $n$  corresponds to the number of electrons involved in the reduction of a single molecule of oxygen,  $k$  is the rate constant for the reduction process,  $F$  is the Faraday constant (96500 C/mol),  $\omega$  is the rotation rate of the electrode (revolution/s).  $D_o$ ,  $C_o$  and  $\nu$

are the diffusion coefficient, bulk concentration and kinematic viscosity of the oxygen molecule respectively. The corresponding values  $D_o$ ,  $C_o$  and  $\nu$  in 0.5 M KOH are  $(1.65 \times 10^{-5} \text{ cm}^2/\text{s})$ ,  $(0.84 \times 10^{-6} \text{ mol}/\text{cm}^3)$  and  $(0.01 \text{ cm}^2/\text{s})$  respectively.

$$\frac{1}{i} = \frac{1}{i_k} + \frac{1}{i_d} \quad (2)$$

$$\frac{1}{i} = \frac{1}{nFkC_o} + \frac{1}{0.62nFD_o^{2/3}\nu^{-1/6}C_o\omega^{1/2}} \quad (3)$$

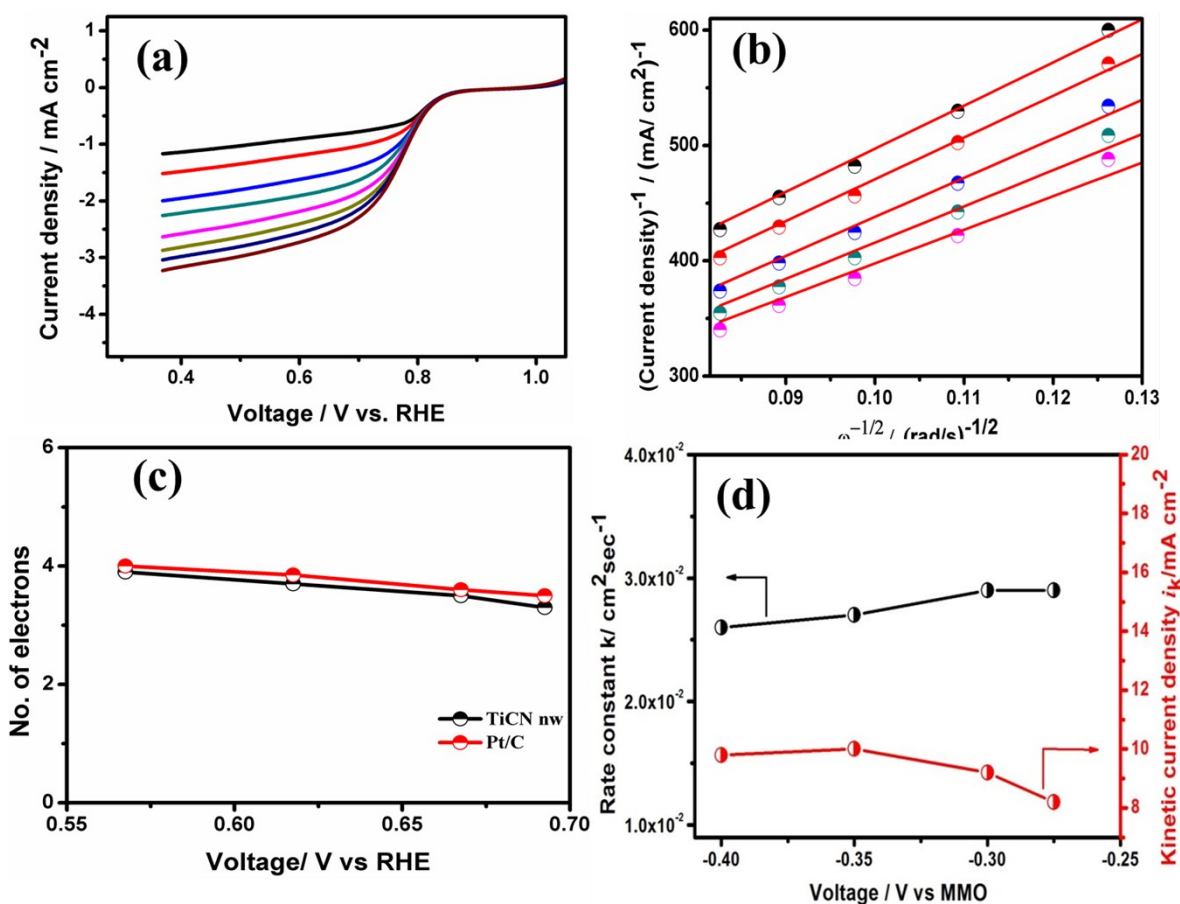


Figure S-6: (a) Linear sweep voltammetric data for ORR on TiCN nanowires in 0.5 M KOH at different rotation rates. (b) corresponding Koutkey–Levich plots at different potentials. (c) no. of electrons determined at different potentials for Pt/C (red), TiCN (black) (d) current density and rate constant as a function of applied bias.

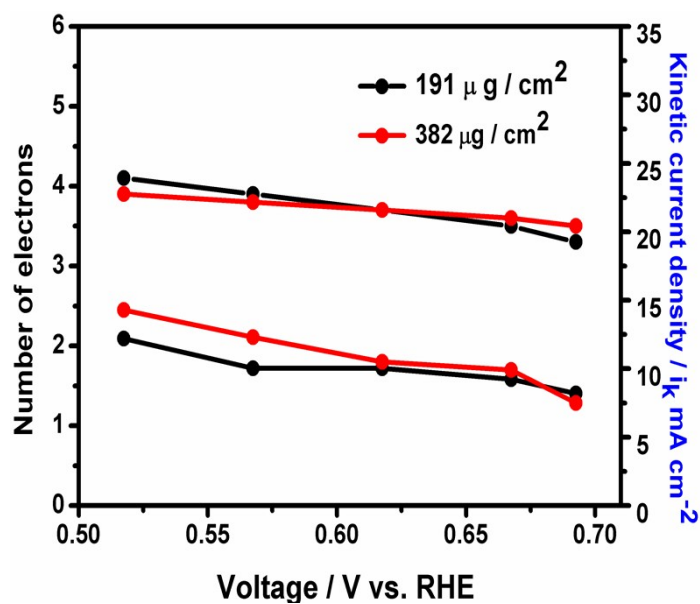


Figure S-7: Effect of different loading of TiCN nanowire on kinetic current density and number of electrons.

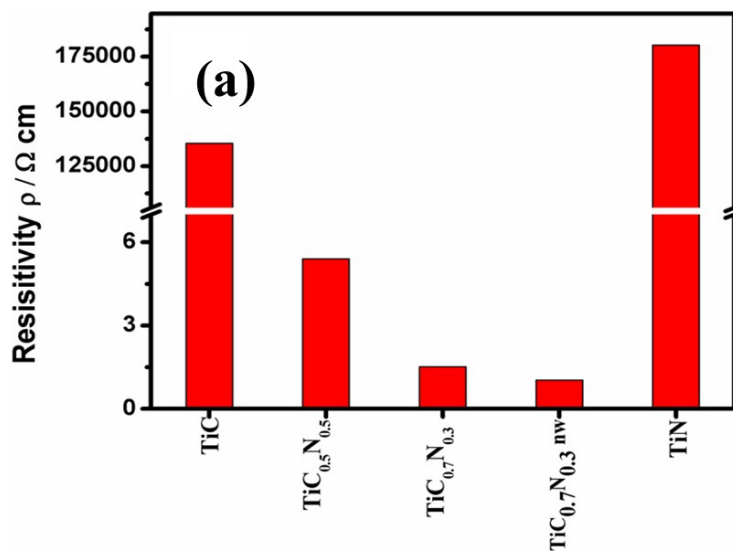
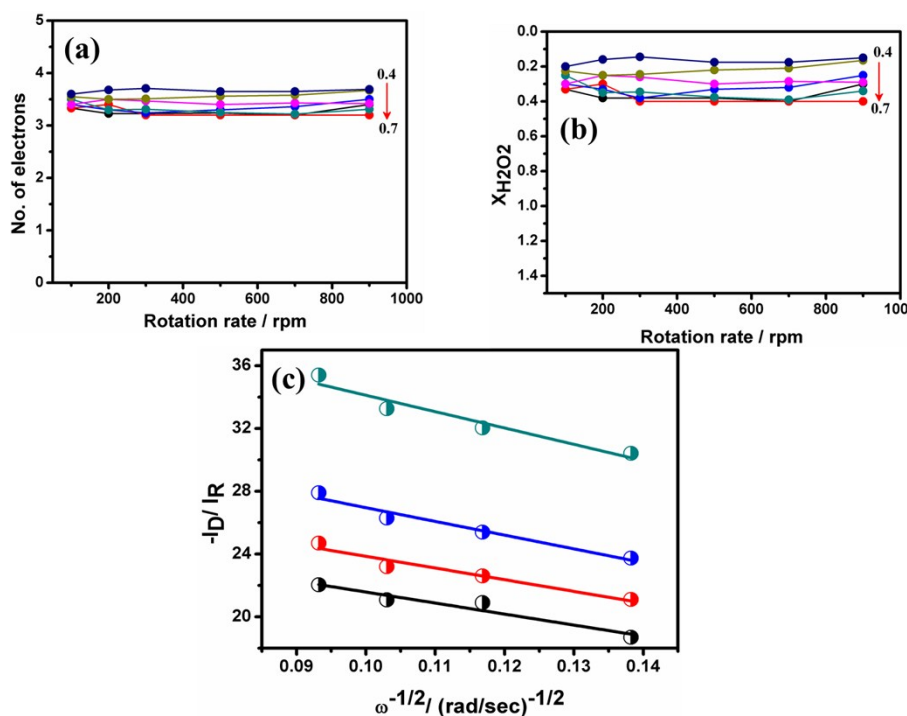


Figure S-8. (a) Resistivity of TiC, TiC<sub>0.5</sub>N<sub>0.5</sub>, TiC<sub>0.7</sub>N<sub>0.3</sub> particles, TiC<sub>0.7</sub>N<sub>0.3</sub> nanowires and TiN.

Rotating ring disk electrode (RRDE) were used to calculate the number of electrons and the amount of  $H_2O_2$  involved in the reduction of oxygen molecule based on the ratio of disk and the ring current as shown in equation 4 and 5 . The procedure used for the RRDE experiments given in experimental section. The obtained result from the RRDE experiments were plotted and is given in Figure S9.

$$n_e = \frac{4I_D}{I_D + \frac{I_R}{N}} \quad (4)$$

$$x_{H_2O_2} = \frac{2I_R}{I_R + NI_D} \quad (5)$$

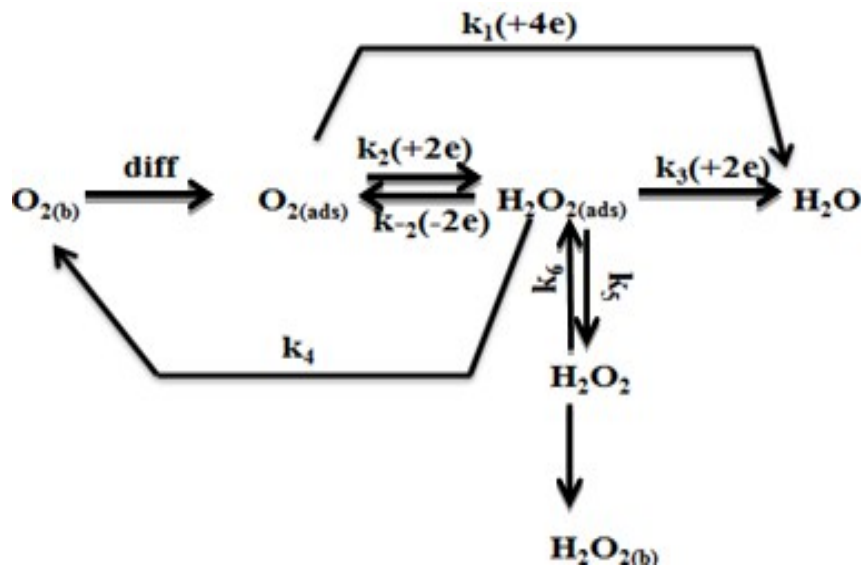


**Figure S-9.** (a) Variation of no. of electrons for different roation rates at different potentials as calculated from RRDE data (b) Yield of production of  $H_2O_2$  at different potentials as determined from RRDE data (c) Plots of  $(I_D/I_R)$  vs  $\omega^{-1/2}$  .

Using method given by Wroblowa et al.<sup>2</sup> it is possible to have an idea about the kinetics of the two pathways of ORR as shown in scheme S1. According to this method plot of  $(I_D / I_R)$  vs.  $\omega^{-1/2}$  gives straight line with different slopes and intercepts at different potentials and is as shown in Figure S9 (c). The obtained slopes and intercept are linear to each other according to equation 6.

$$J = \frac{1}{N} [1 + (2k_1 / k_2) + (SZ / k_6)] \quad (6)$$

In the equation J is the intercept, S is slope and Z correspond to constant which is equals to  $0.62D^{2/3}\nu^{-1/6}$ .



**Scheme S1: Reaction scheme given by Wroblowa et al. showing different pathways involved in ORR,  $k_1$  corresponds to the direct conversion of oxygen to water and  $k_2$  corresponds to the reduction of oxygen via  $H_2O_2$ .**

Stability is one of the important parameters should be looked at for a catalyst when it has to be integrated in devices. The stability of the catalyst had been studied by cycling the system in an O<sub>2</sub> saturated KOH for 1000 cycles. The plot of peak current density vs. cycle numbers is given in Figure S12 (a). Almost 90% of the activity of the system is retained even after 1000 cycles shows the stability of the catalyst. This stems from the inherent stability of the catalyst against corrosion. Further to check the material retains its morphology we dispersed the electrode material in isopropanol by sonication for 5 minute in the respective solvent and drop casted on silicon substrate. Scanning electron microscopic (SEM) image (Figure S12 (b)) of the sample shows TiCN retain its nanowire morphology after the experiment. Further a chronoamperometric study has been performed to test the stability of the catalyst by holding at a potential of 0.82 V vs. RHE and the variation in current was monitored for 10 hrs. The catalyst could

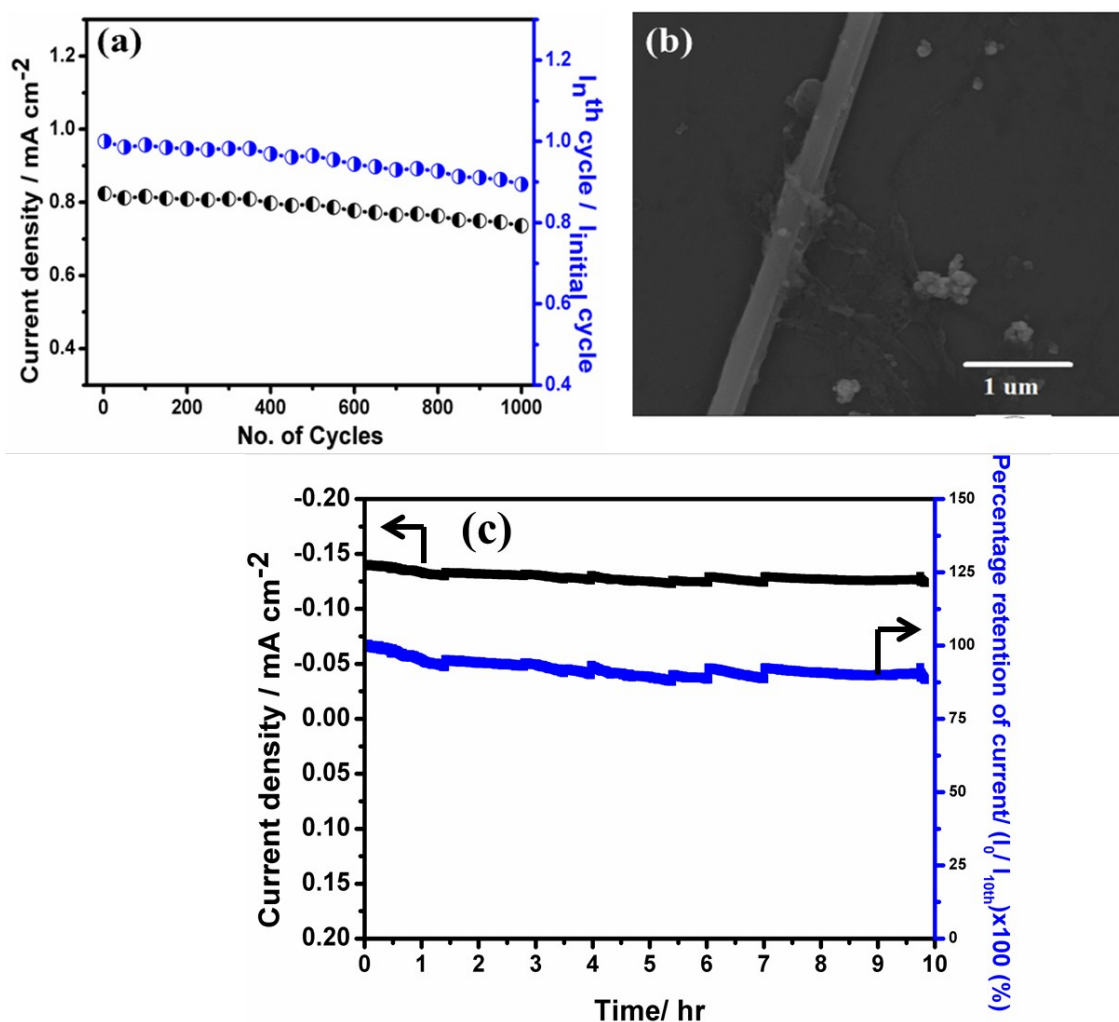


**Figure S-10 (a) Variation of peak current density as a function of cycle number. (b) SEM image of the sample taken after cycling the electrode for about 1000 cycles. (c) Chronoamperometric study held for 10 hrs by holding the potential at 0.82V**

**Zinc-air battery – Primary:**

To test the primary Zinc battery performance with TiCN nanowire as cathode was done by carrying out at discharge at different drain currents like 5, 20, 50, 100 and 200 mA/ cm<sup>2</sup> until the entire zinc foil (anode) is consumed. The specific capacity is calculated based on the mass of consumed Zn (Figure S11b). The experiments have also been performed in air breathing mode (without purging oxygen) at constant discharge current of 20 mA/ cm<sup>2</sup> (Figure S11d). It is observed that the cell runs with a potential close to 1.1 V vs. Zinc for several hours.

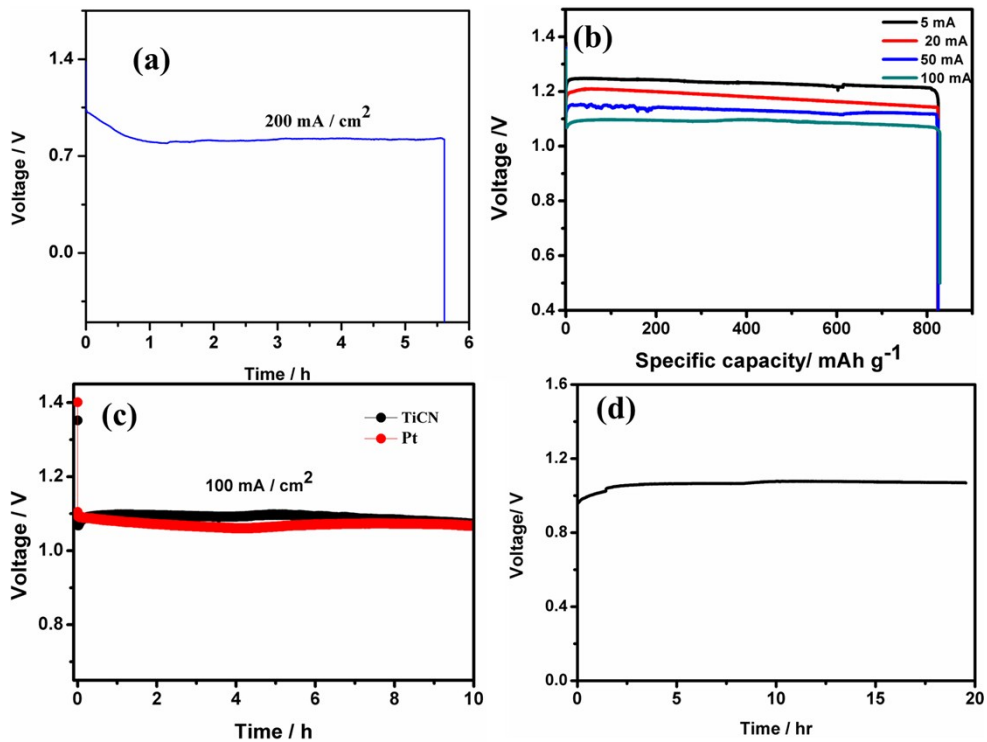


**Figure S-11. (a) Discharge curve at 200 mA/cm<sup>2</sup> (b) Plot of specific discharge capacity normalized to the mass of consumed zinc at different drain currents. (c) galvanostatic**

discharge of primary zinc air battery using TiCN as cathode catalyst at current density of 100 mA/cm<sup>2</sup> compared with Pt/C catalyst at the same current density. (d) Long term discharge curve of zinc air battery with a drain current of 20 mA / cm<sup>2</sup> in air breathing mode.

Stability of TiCN cathode has been checked by monitoring the X-ray diffraction patterns before and after discharge experiment. Figure S12 illustrates the XRD patterns of TiCN nanowires before and after galvanostatic discharge experiments and are found to be the same. The electrodes after the discharge experiments are washed thoroughly with deionized water prior to recording XRD.

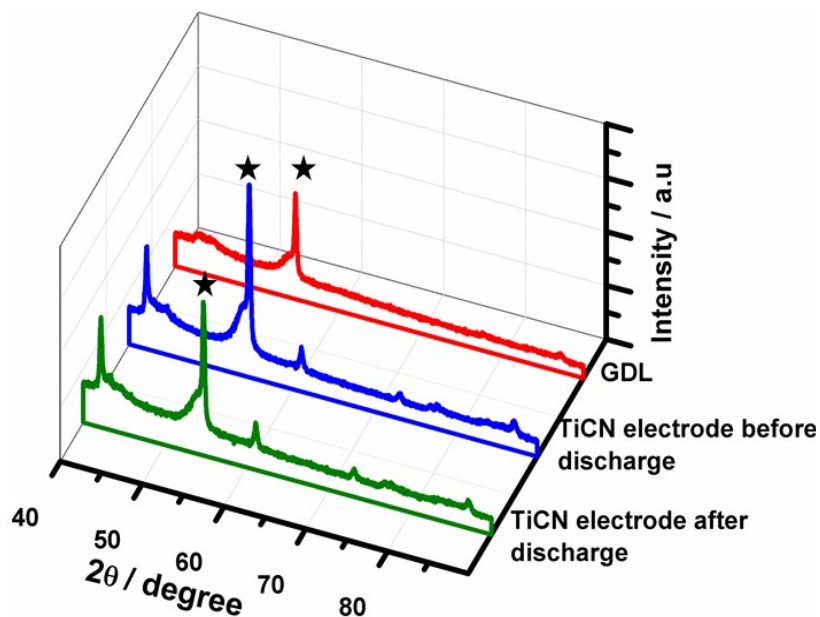


Figure S-12. XRD pattern GDL (red), TiCN loaded GDL before (blue) and after (green) discharge.

### Rechargeable batteries

For Rechargeable zinc air batteries, we have used TiCN as ORR catalyst and IrO<sub>2</sub> as oxygen evolution (OER) catalyst. In the present study, we have employed three-electrode

configuration in which ORR and OER catalysts are coated onto two separate electrodes and kept parallel to each other. The zinc anode is placed between these two electrodes.

While charging, to facilitate electro-deposition of zinc on anode, additional 0.2 M zinc acetate salt is added to 6 M KOH. Figure 5b and S13 illustrate the cycling performance of rechargeable zinc air battery at current rates of 50 mA /cm<sup>2</sup> and 20 mA /cm<sup>2</sup> for the 2 and 8 hour cycle period respectively. A flat voltage plateau is observed in both low and high current ranges for entire operation time. For a drain current of 20 mA / cm<sup>2</sup>, the potential difference between charge and discharge plateau is about 0.8 V whereas for a current density of 50 mA, it is found to be 0.87 V. In addition, the round trip energy efficiencies for 20 mA and 50 mA current densities are found to be around 60 % and 56 % respectively.

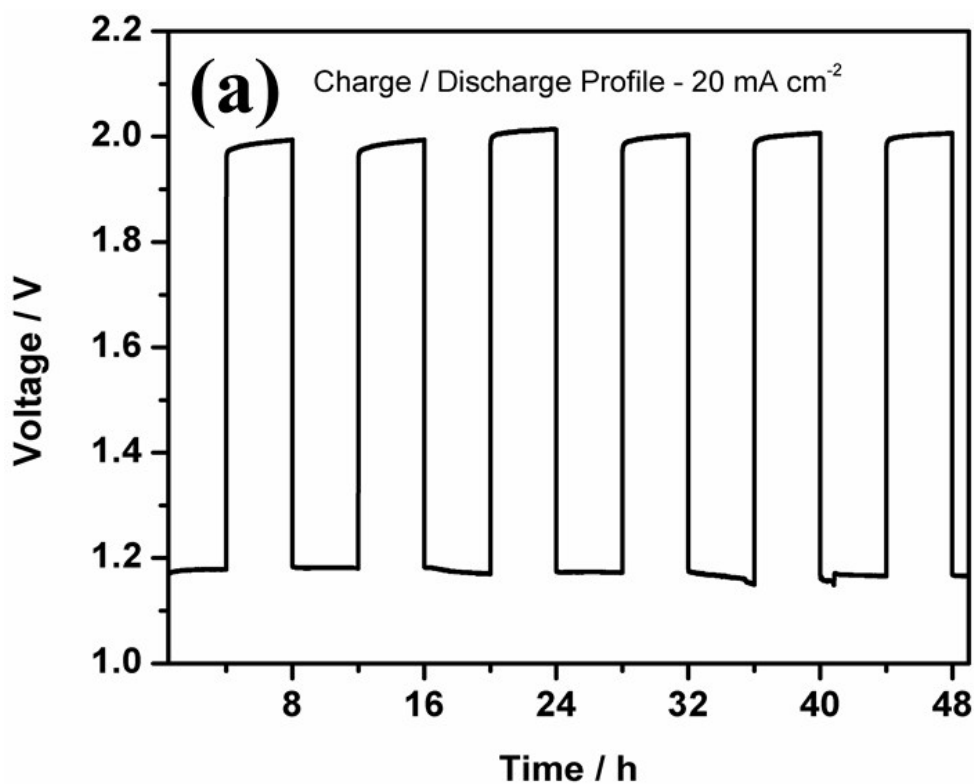


**Figure S-13. Charge – discharge cycle at 20 mA/cm<sup>2</sup> for the rechargeable battery with three electrodes of TiCN for ORR and IrO<sub>2</sub> for OER and Zn anode (8 h. cycle period).**

Electrocatalyst for ORR	Catalyst Loading (mg/cm <sup>2</sup> )	Current density@ 0.6 V (mA/cm <sup>2</sup> )	Maximum Power density, (mW/cm <sup>2</sup> )	Reference
TiCN nanowire	1	470	281	Present work
CoO/N-CNT	1	420	265	<i>Nat. Comm.</i> <b>2013</b> , 4, 1805-1810
MnO <sub>2</sub> /Co <sub>3</sub> O <sub>4</sub>	2	55	33	<i>Nanoscale</i> , 2013, 5, 4657-4661. (35 a)
α-MnO <sub>2</sub> -LaNiO <sub>3</sub> -CNT	-	100	55	<i>RSC Adv.</i> 2014, 41, 46084-46092.(35 b)
Active graphenenanosheets	0.7	50	42	<i>J. Electrochem. Soc.</i> 2013, 160, F910-F915. (35 c)
Ag/C nanoparticles	30	@35 °C, 90 @85 °C, 120	@35 °C, 30 @85 °C, 70	<i>J. Power Sources</i> , 2009, 193, 885-889. (35 d)
rGO-Mn <sub>3</sub> O <sub>4</sub>	Activated carbon 62 wt% + 8 wt% catalyst	190	120	<i>Energy Environ. Sci.</i> 2011, 4, 4148-4154.(35 e)
N-doped CNT	0.2	130	75	<i>Electrochem. Acta</i> , 2011, 56, 5080-5084. (35 f)

**Table S-4: Comparison of different key parameters obtained for TiCN as cathode catalyst in primary Zn-air cell with earlier reported literature values<sup>3</sup>**

Ag-Cu alloy	0.1	100 (@0.8V)	82.1	<i>ACS Appl. Mater. Inter.</i> <b>2015</b> , 7, 17782-17791
-------------	-----	----------------	------	--

### Gel Based Zinc-Air batteries

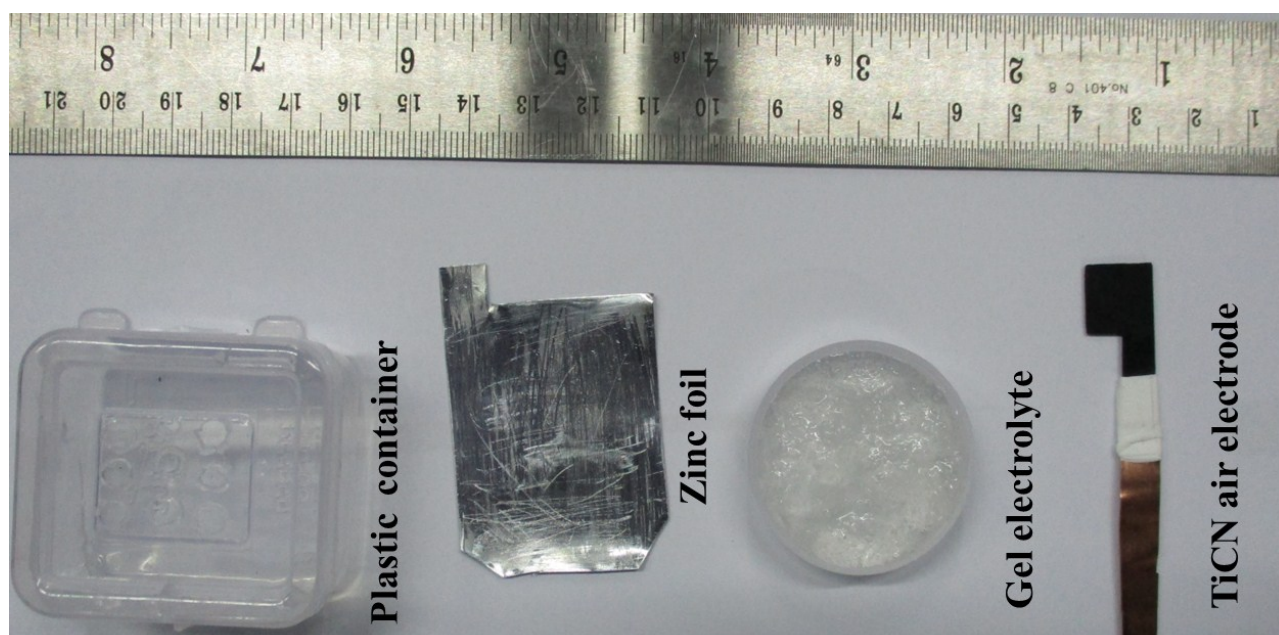


**Figure S-14:** Gel based zinc cell used for testing the primary Zn-air battery with an inlet for oxygen supply. i) Plastic container ii) Zinc foil iii) Gel electrolyte iv) TiCN catalyst loaded ( $1\text{mg}/\text{cm}^2$ ) on GDL.

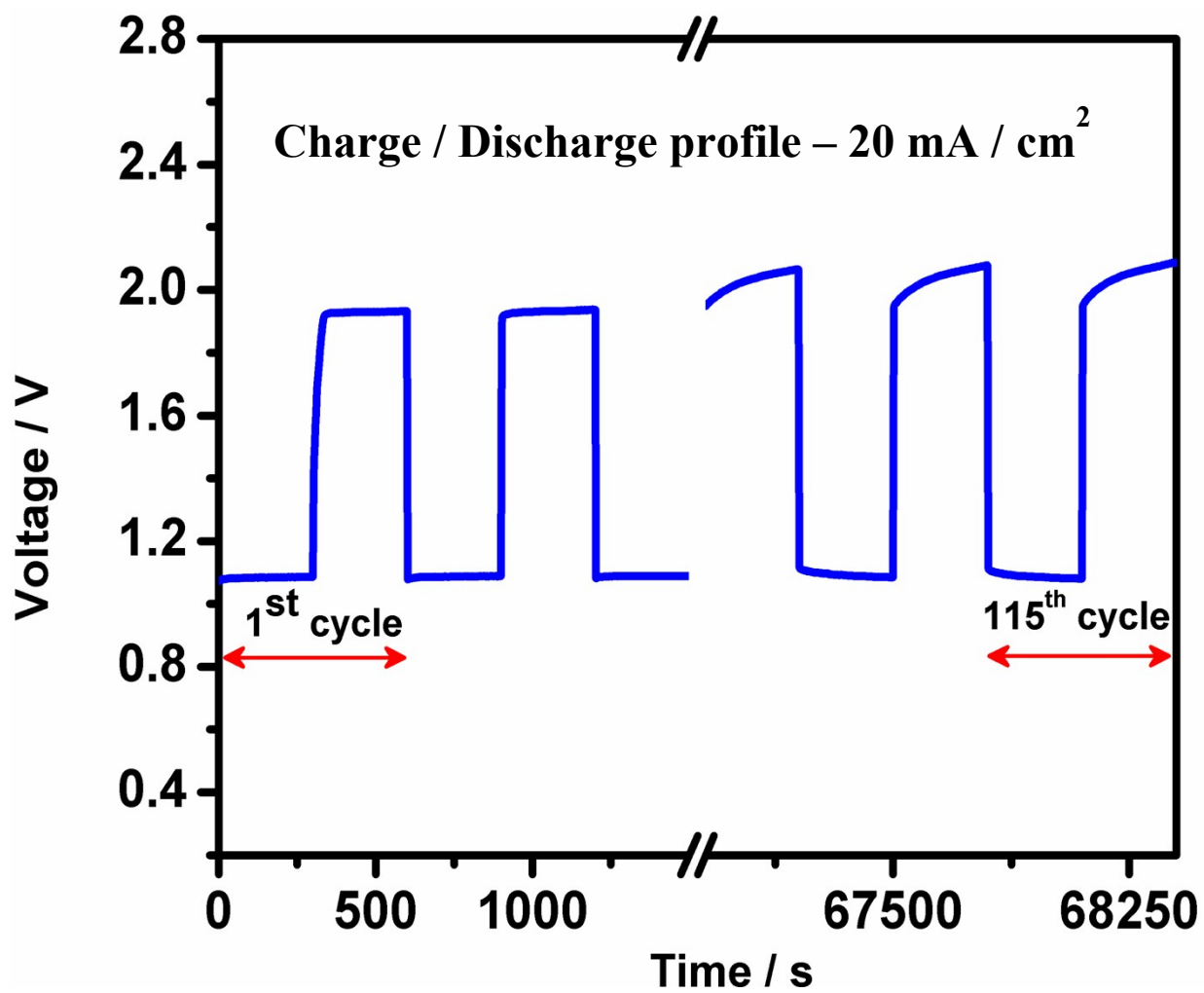
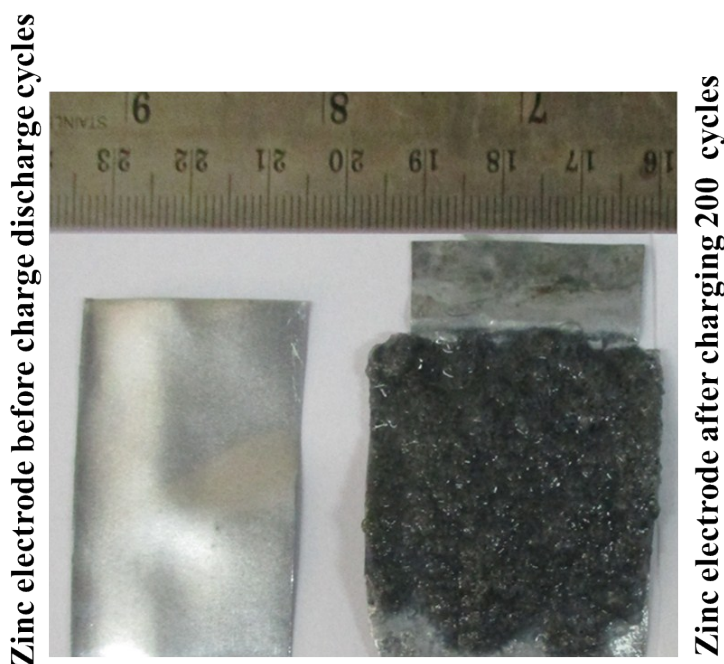


Figure S-15. Charge/discharge profile for a period of 10 h at 20 mA/cm<sup>2</sup> current density in the three configuration as given earlier.

After charge - discharge (200) cycles in the gel electrolyte, the zinc electrode is taken out, washed carefully and checked (Figure S18). There is clear deposition of zinc on the zinc foil facing the OER catalyst and dissolution of zinc happens on the other side.



**Figure S-16. Photograph of the zinc electrode and the zinc foil facing to the OER catalyst after charging.**

### References:

- 1 a) M. D. Segall, J. D. L. Philip, M. J. Probert, C. J. Pickard, P. J. Hasnip, S. J. Clark, M. C. Payne, *Journal of Physics: Condensed Matter* 2002, 14, 2717. b) J. P. Perdew, K. Burke, M. Ernzerhof, *Physical Review Letters* 1996, 77, 3865-3868. c) H. J. Monkhorst, J. D. Pack, *Physical Review B* 1976, 13, 5188-5192.
- 2 .H. S. Wroblowa, Y. C. Pan, G. Razummey, *J. Electroanal. Chem.* 1976, 69, 195-201.
3. a) G. Du, X. Liu, Y. Zong, T. S. Andy Hor, A. Yu, Z. Liu, *Nanoscale* 2013, 5, 4657-4661. (b) H. Ma, B. Wang, *RSC Adv.* 2014, 41, 46084-46092. (c) D. U. Lee, H. W. Park, D. Higgins, L. Nazar, Z. Chen, *J. Electrochem. Soc.* 2013, 160, F910-F915. (d) J. J. Han, N. Li, T.Y. Zhang, *J. Power Sources* 2009, 193, 885-889. (e) J. S. Lee, T. Lee, H. K. Song, J. Cho, B. S. Kim, *Energy Environ. Sci.* 2011, 4, 4148-4154. (f) S. Zhu, Z. Chen, B. Li, D. Higgins, H. Wang, H. Li, Z. Chen, *Electrochem. Acta* 2011, 56, 5080-5084.